CHAPTER 4

FAN BLADE DAMAGE DETECTION

4.1 Introduction

From the results obtained in Chapter 2 with the FEM of various blade models, it was clear that it is viable to detect damage using one sensor per blade (possibly less) by making use of the shift of natural frequencies due to structural changes. The purpose of the EFBDS was to verify these findings experimentally, using a model that simulates the conditions that will be found on an actual fan as described in Chapter 3. This chapter concentrate on the measurements taken from the EFBDS and the results obtained.

A brief description of the experimental conditions, sensors and processors used is given. The next step was to look at the effect of certain variables such as rotation speed, blade pitch and sensor type and location. Thereafter the signal conditioning and reasons for the conditioning, the measurement period and number of measurements was studied. This was evaluated by looking at the feature extraction results obtained from ARMA models. As described in Chapter 1 it was important that a specific natural frequency could be determined accurately and repeatedly. The main reason for this being the relatively small shifts of frequency for low levels of damage and the need to distinguish between measurement inaccuracies and shifts due to damage. With these variables fixed, different levels of damage was induced to the structure to ascertain the selection criteria and classification structure.

Time domain damage indicators such as Root Mean Square (rms) values, Kurtosis, Crest factors and variance were also evaluated as a possible means of damage identification with future work that may include neural networks in mind.

The only remaining step was then to compare the predictions of the finite element model to the experimental results found with the EFBDS. This included updating of the finite element model if necessary.

4.2 Experimental conditions

The following measurement equipment were used for all experimental measurements:

Table 4.1: Description of measurement equipment

Name	Description
1 x PCB 100 mV/g Accelerometer	353B65
1 x PCB 10mV/g Accelerometer	352C22 Shear accelerometer.
2 x PCB strain gauges.	740B02 piezoelectric strain gauge.
1 x Siglab	Model 20-22 Signal analyser
4 x Signal conditioners	480E09 Battery-powered signal conditioners
1 x Personal Computer.	Pentium ™ 200MMX, 64M RAM.

4.2.1 Placement of sensors

Two different types of sensors were used. The first sensor type used, was a piezoelectric accelerometer, while the second sensor type was a piezoelectric strain gauge. Because of the different physical measurements these sensors make, the optimal location of measurement is not always the same.

The finite element model provided valuable insight regarding the placement of the sensors at a position where the third and fourth mode shapes cause maximum strain or acceleration, depending on which type of sensor was used. To find a suiTable location for the accelerometer, an analysis was done to give a displacement plot of the third and fourth modes shapes. These plots can be seen in Figure 4.1 and 4.2.

As can be expected, it is better to place the accelerometer as far out towards the tip of the blade as possible. Because the fourth mode shape is a torsional mode, the nodal points (position of zero movement) lie along the middle of the blade. It was necessary to offset the sensor to the left or right side of the centreline of the blade to make sure this mode can be measured as indicated in Figure 4.1. In the same way, the maximum strain occurs at the root of the blade. Again, the sensor should be offset from the centreline to measure the fourth mode shape.

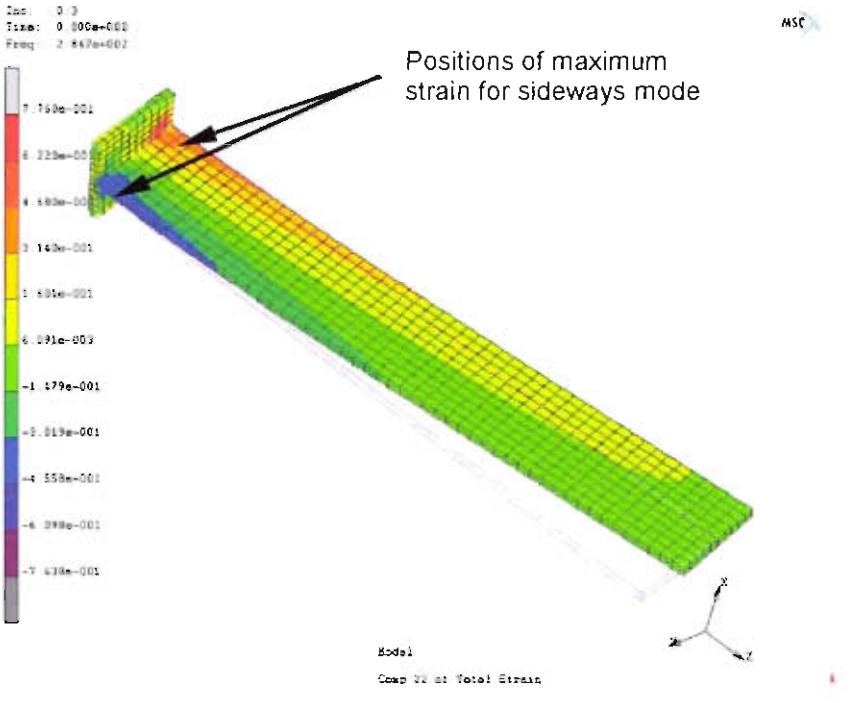

Figure 4.1: Optimal strain location in the y-y direction for third mode shape

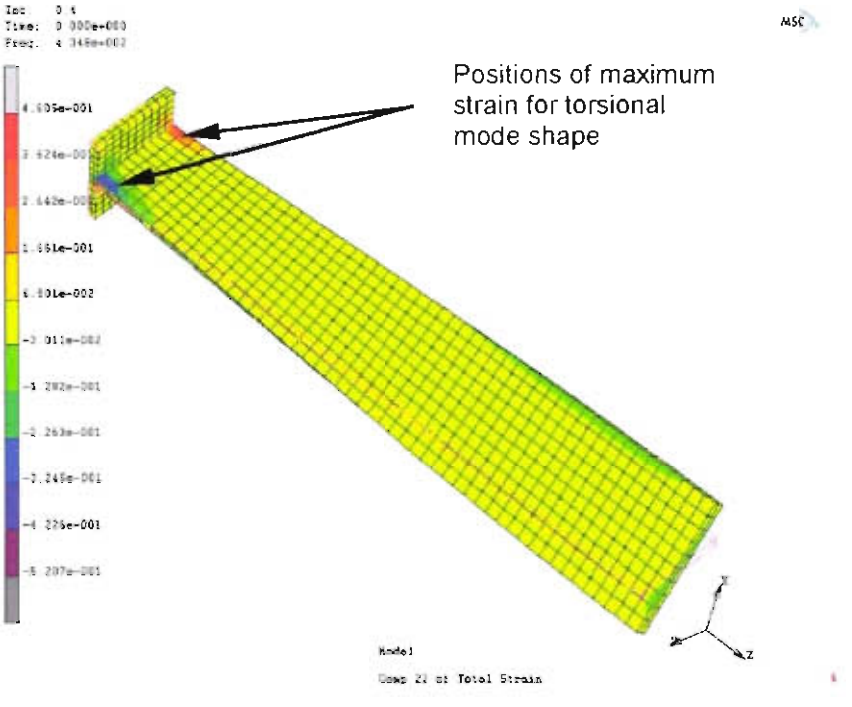

Figure 4.2: Optimal strain location for the fourth mode shape

4.2.2 Typical results obtained

To test the ability of the ARMA model to correctly identify model parameters and get some idea of what settings should be used for this algorithm, a simple aluminium cantilever beam was analysed. An electromagnetic exciter was used to provide stochastic input to the system and only output data from an accelerometer was measured for use with the ARMA algorithm. The details of the tests conducted can be seen in Appendix C.

As can be expected, the Power Spectral Density (PSD) found on the blades is not as well defined as those found on a stationary cantilever beam. In particular, the blade pass frequency and its harmonics was very prominent. Furthermore, the speed control system of the three phase electrical motor caused further electromagnetic noise. Even though the resulting PSD was less than ideal, repeaTable results could be obtained by ARMA curve fits. An example of an ARMA fit for an accelerometer can be seen in Figure 4.3, while Figure 4.4 shows a typical piezoelectric strain gauge fit.

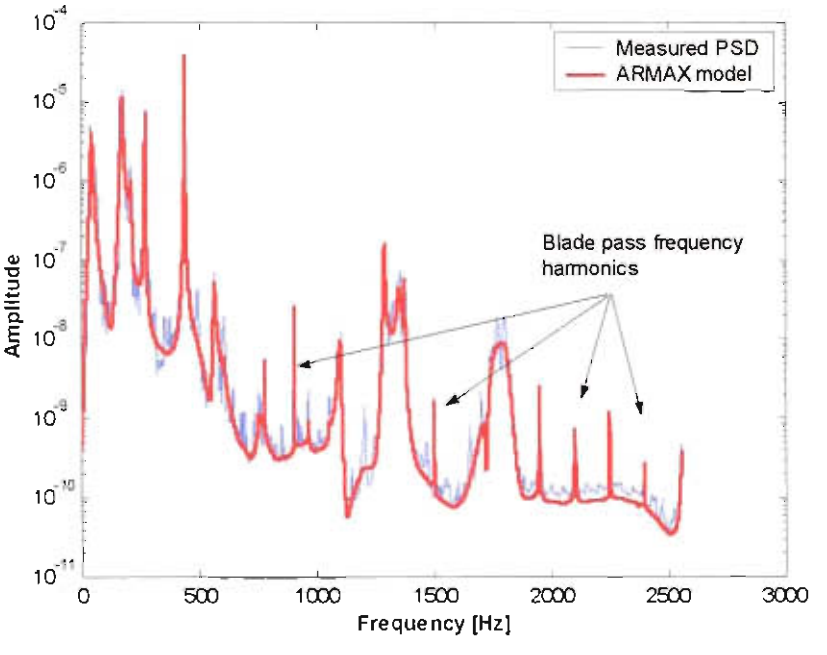

Figure 4.3: Typical ARMA fit to accelerometer data, note blade pass frequency harmonics

As can be expected the blade pass frequency harmonics result in a very narrow band excitation, while the natural frequencies result in a broader band, higher power distribution. Natural frequencies can be seen at around 200 Hz, 280 Hz, 440 Hz, 560 Hz, 1100 Hz, 1340 Hz and 1800 Hz. The peak at 75 Hz corresponds to the blade pass frequency. The rotational velocity for this measurement case was

750 r.p.m., translating to 12.5 Hz. Due to the six stationary support beams of the structure, the blade pass frequency will then be at 75 Hz.

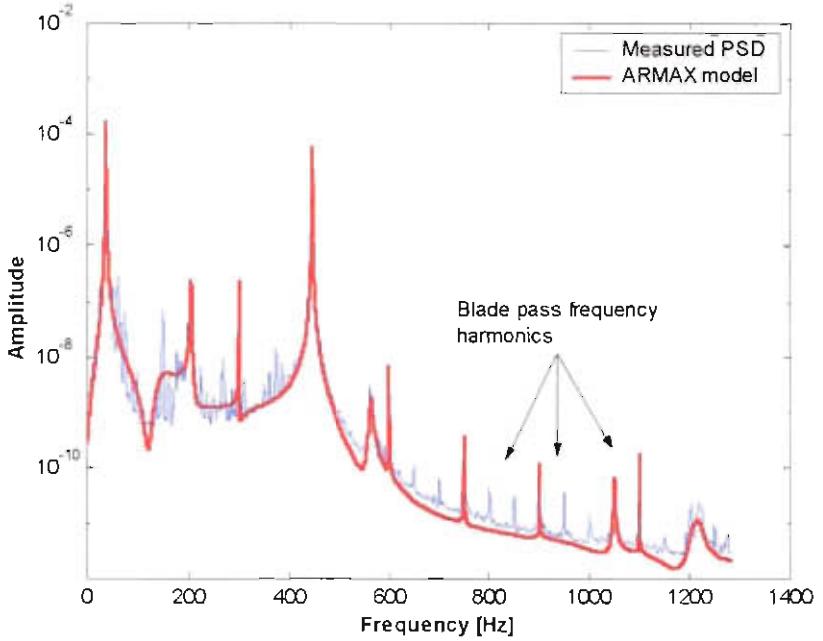

Figure 4.4: Typical ARMA model fit to piezoelectric strain gauge, note blade pass frequency harmonics

For the measurement in Figure 4.4 the distance between these excitation peaks on the x-axis (frequency) was found to be approximately 45 Hz. This corresponds to 6 times the rotational speed (in this case 450 r.p.m.). This was again due to the six stationary support structures found on the EFBDS (see Chapter 3).

Although these harmonic frequencies make it necessary to fit a higher order ARMA model in order to make sure all the natural frequencies are found, it was possible to work with the data obtained. A blade pass frequency can be expected on an actual fan, and the technique for the detection of damage developed, must be robust enough to handle these various noise sources found in the spectrum.

Another source of noise was the speed control system used for the three-phase motor. This caused a broad band noise floor to be present. To demonstrate the effect this noise has on the spectrum a 4 s measurement was taken at 600 r.p.m. and compared to a 4 s measurement taken just after the controller was shut down at 750 r.p.m. The results can be seen in Figure 4.5 on the next page.

As can be seen, the effects of the blade pass frequency were also greatly reduced. The fan loose momentum quite quickly because of air resistance and thus the blade pass frequency change rapidly from around 75Hz to 45Hz (4s at 18° pitch angle).

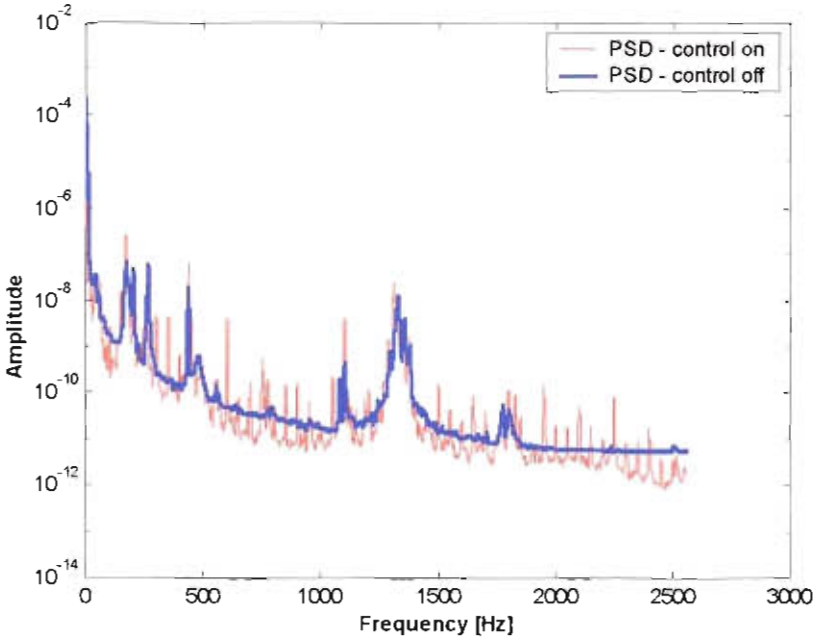

Figure 4.5: PSD with speed controller operating (red), and coasting to stop (blue).

While measurements taken during run-downs were substantially cleaner and required a lower order ARMA model for an accepTable fit, it was not really practical since an actual fan is not switched off unless maintenance is required. Furthermore almost any fan will have a blade pass frequency in practice and any technique developed for the detection of damage in fan blades should be able to cope with such noise.

Another variable of the EFBDS was pitch of the blades. Figure 4.6 shows a spectrogram of channel 2, taken at 500 Hz sampling frequency at pitches of 0°, 27° and 45°. Clearly energy input (and response) get higher with increasing pitch. The blade pass frequencies also became more prominent with increasing pitch. Figure 4.7 shows the ARMAX fits and the general noise level of measured PSDs at different pitch levels. If too little stochastic excitation was present (0° pitch), the natural frequencies did not get excited enough to stand out clearly from electric and other noise. While the second and fourth natural frequencies were not very sensitive to the pitch angle, the third was very sensitive. FEA results confirmed that the second mode shape is very sensitive to pitch angle. The blade pitch angle was therefore locked at 18° for all subsequent measurements so as not affect measurements.

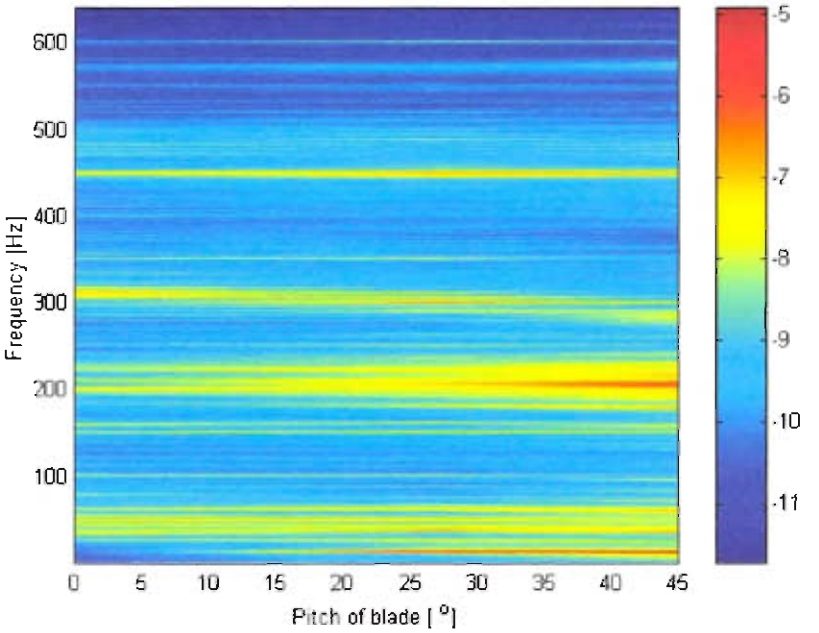

Figure 4.6: Spectrogram showing increase of response with increasing blade pitch

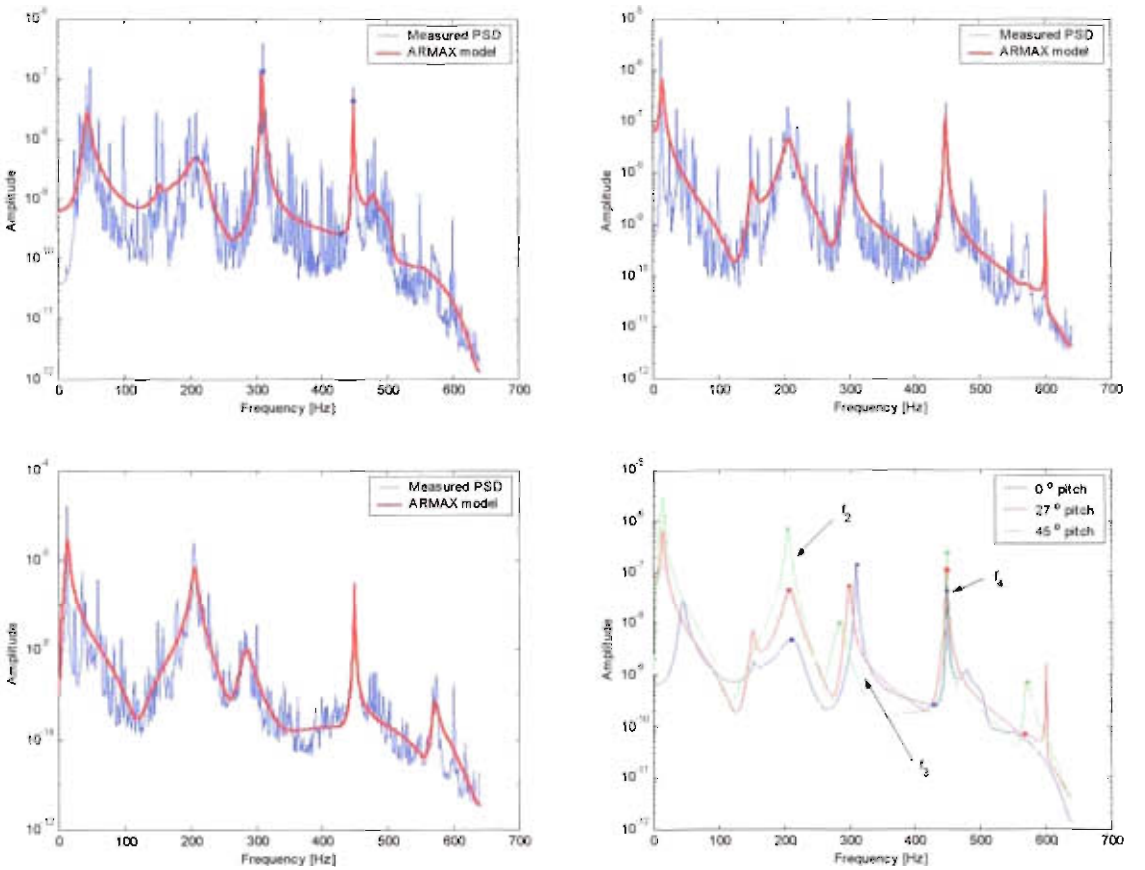

Figure 4.7: Top left at 0°, top right at 27°, bottom left at 45°, bottom right, comparison

4.3 Experimental results

The ARMA model algorithm used time signal data as input although this algorithm eventually fitted a polynomial through a power spectral density plot for modal parameter extraction purposes.

4.3.1 Processing of raw data

An example of a 2 s measurement, sampled at 500 Hz can be seen in Figure 4.8. The most apparent characteristic of this measurement was the one times rotational frequency sine wave found because of imbalance in the system. A six times rotation frequency is superimposed on this signal, followed by al the other frequencies present in this system. Since the first natural frequency was found to be around 33 Hz during the finite element analysis, it was decided to high pass filter the signal from 25 Hz. The filtered signal can be seen in Figure 4.9.

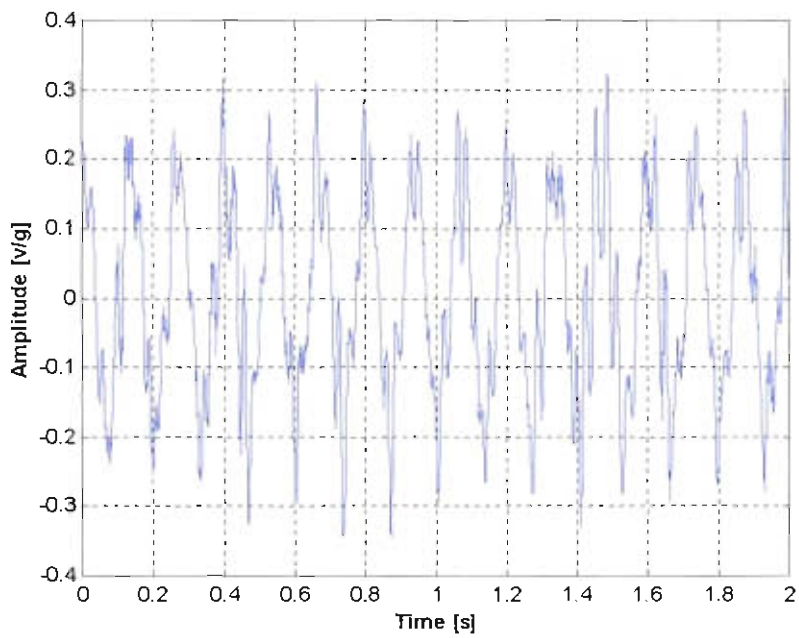

Figure 4.8: Example of the typical time data measurement (f_s was 500Hz).

The primary reason for filtering the signal was to lower the order of the ARMA model required to fit an accurate polynomial. Since the first natural frequency that could be measured accurately and showed relatively high sensitivity to damage was found at around 280 Hz, filtering below 200 Hz was also implemented. The ARMA algorithm struggled to fit repeaTable curves through the resulting power spectral density how-

ever and the order of the model could not be decreased as a result. It was thus decided not to filter to such a high frequency.

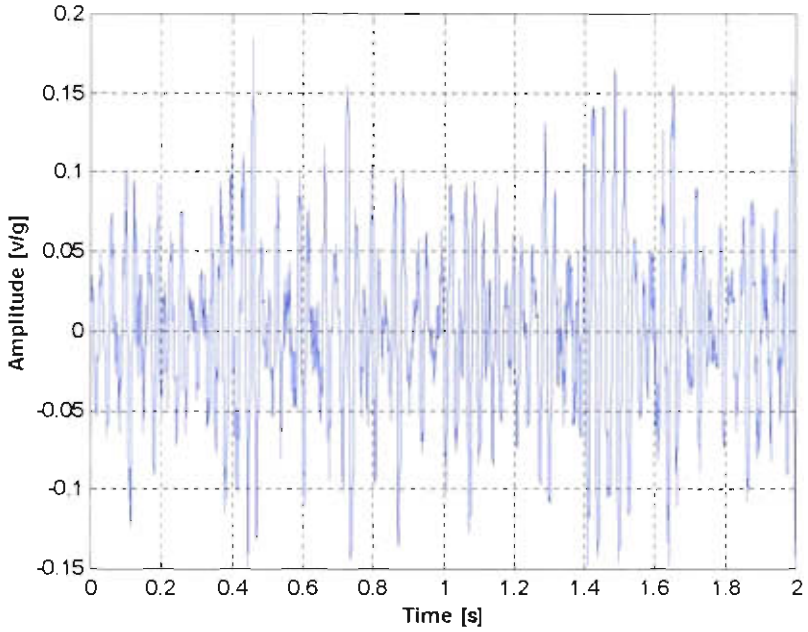

Figure 4.9: The filtered signal, note change of maximum amplitude

4.3.2 Determination of required order for ARMAX curve fits

As discussed in Appendix C, a certain minimum model order was necessary for the ARMAX model. The pole-zero plots for a number of typical measurements can be in Figure 4.10 for 500 Hz sampling, Figure 4.11 for 1000 Hz sampling frequency and Figure 4.12 for 2000 Hz sampling frequency.

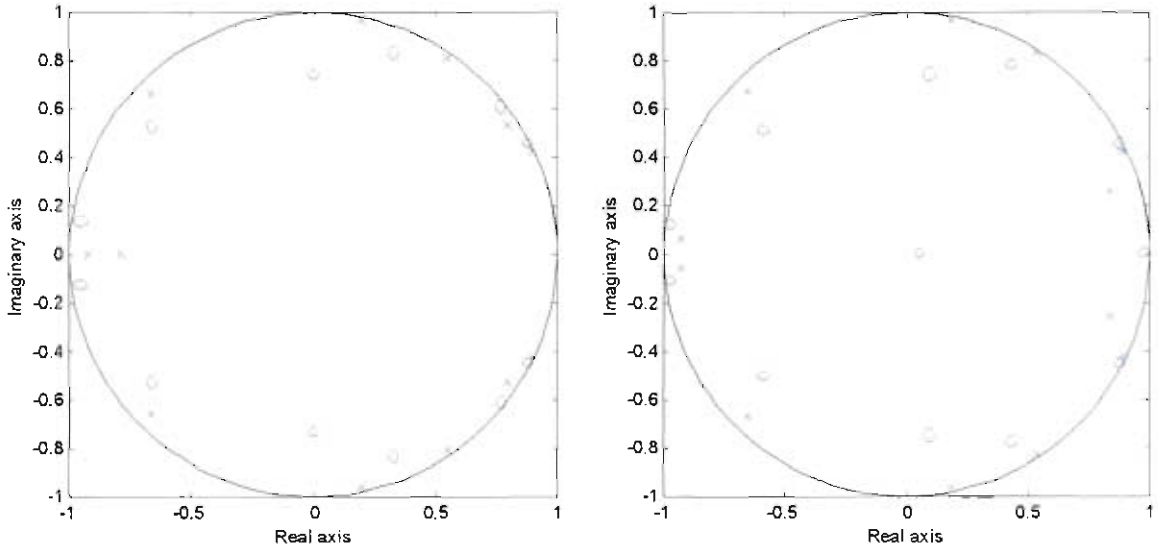

Figure 4.10: Pole-zero plot for a 2 s (left) and 4 s fit (right)

It was clear that a few near redundant poles were present (proximity of poles and zeros). Appendix C deals with the implication of this phenomenon in more detail. Due to the high level of noise (blade pass frequency and electromagnetic) this was necessary to ensure all the natural frequencies were picked up.

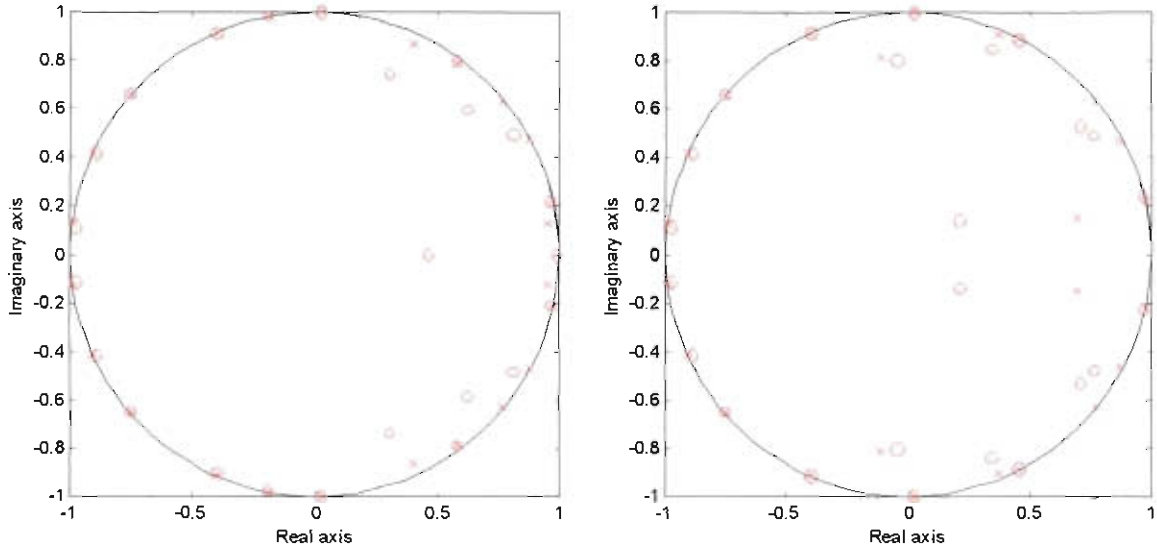

Figure 4.11: Pole-zero plot for a 2 s (left) and 4 s fit (right)

Clearly the number of redundant poles increased dramatically for higher sampling frequencies. The reason for this can be clearly seen in Figures 4.13 and 4.14.

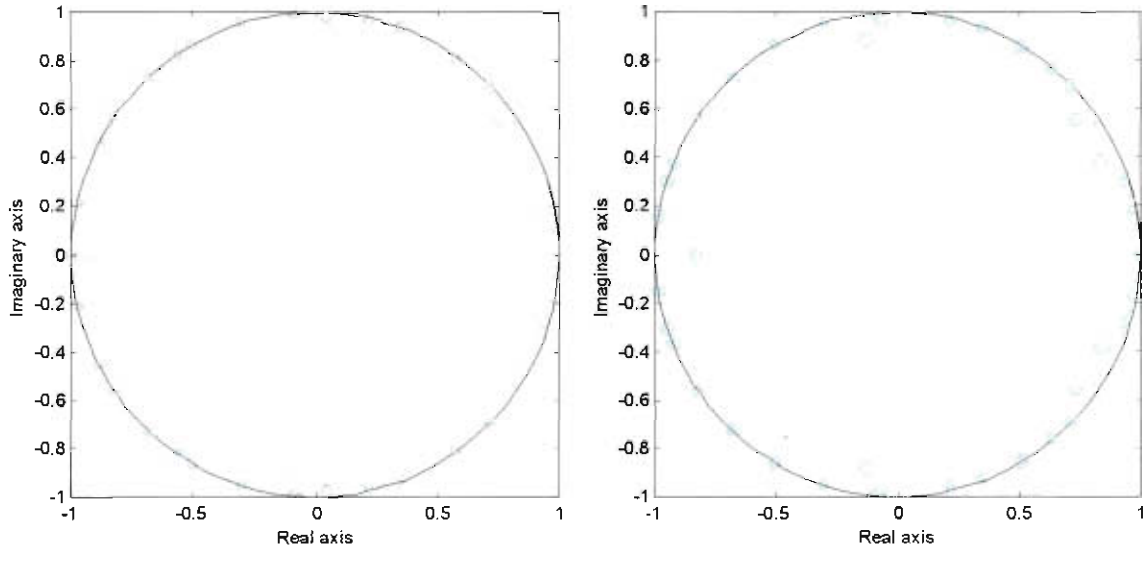

Figure 4.12: Pole-zero plot for a 2 s (left) and 4 s fit (right)

The higher order was necessary because of dominating effect of the noise spectrum from around 600 Hz and up.

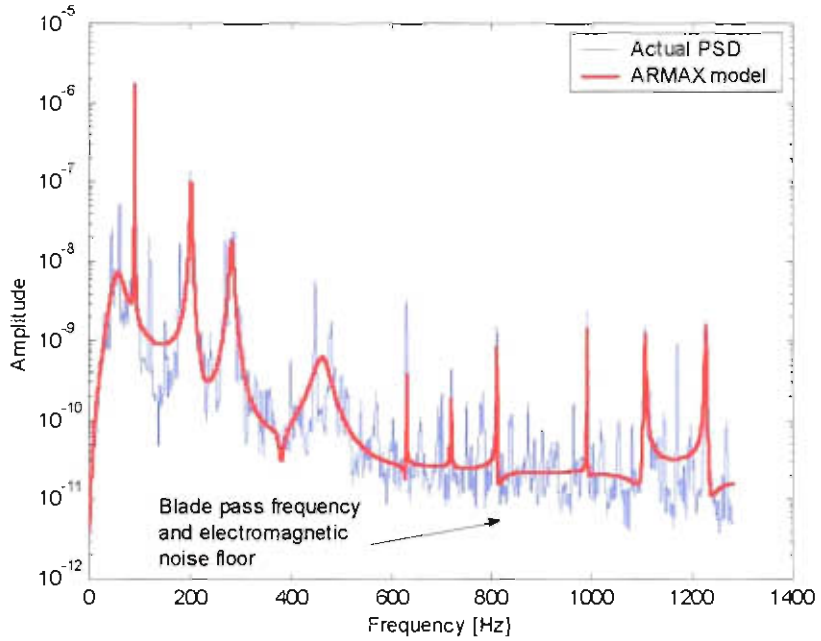

Figure 4.13. Reason for high number of redundant poles and zeros (1000 Hz sampling frequency)

Both of these PSDs were four second samples taken with the 10mV/g accelerometer and represent the worst-case data found during the experimentation phase. Even though these data sets were clearly far from ideal, reliable and repeaTable results could be obtained with the ARMAX algorithm used. A peak picking algorithm was used to identify the natural frequencies.

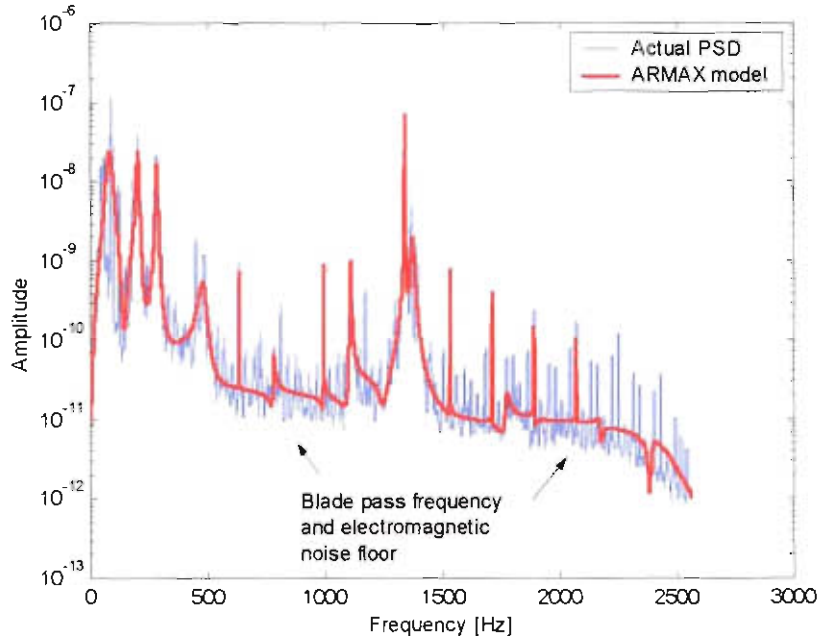

Figure 4.14. Reason for high number of redundant poles and zeros (2000 Hz sampling frequency)

In the end, the order of the model was determined not as much by minimising the number of redundant poles and zeros but by the ability of the ARMAX algorithm to find all the relevant peaks that represented the natural frequencies of the structure. This was only accomplished if the order was increased beyond a certain point. For 500 Hz, a 12^{th} order fit was necessary while 24^{th} and 48^{th} order fits were necessary for the 1000 Hz and 2000 Hz sampling frequency, samples.

4.3.3 Determination of measurement number and length

It was very difficult, if not impossible, to compute the period of time domain data that will be required for an accurate model beforehand. Because the shifts in natural frequencies found for various damage levels are so small, it was very important that natural frequencies could be found repeatedly in an even smaller band of uncertainty. Since the frequency may shift by as little as 0.3% for 10% damage, the error of the measured frequency must then be less than half this shift to ensure accurate classification of the damage level at that frequency. From work done earlier on a simple hinged beam to evaluate the ARMA modelling technique, a rough estimate on the period of measurement and number of measurements was made.

After these initial measurements had been used to compute models, the results could be used in a statistical analysis to make a better estimate of the amount of measurements that would be needed for a certain accuracy to be obtained. Since long time signals combined with high order ARMA models increased computer time dramatically (Appendix C, Tables C.5 and C.6), it was important to minimise the number of measurements and the measurement time.

One method that can be used is confidence intervals (Bendat and Piersol, 1967). If a variable *x(k)* is normally distributed (it will be in this case) with an average value of μ_x and an unknown variance, the sampling distribution for the mean sample $\bar{x}$ will look as follows :

$$\frac{\bar{x} - \mu_x \sqrt{N}}{s} = t_n \qquad \text{n = N - 1} \qquad \textbf{(4.1)}$$

In this case t_n has a normal distribution with n=N-1 degrees of freedom, where N is the number of elements in the sample data set. A probability statement for the sample mean $\bar{x}$ prior to collection of the sample can then be made.

$$Prob\left[\bar{x} > \left(\frac{st_n}{\sqrt{N}}\right) + \mu_x\right] = \alpha \qquad \textbf{(4.2)}$$

For a general case of a normally distributed random variable with an unknown mean value and variance, the probability statement can be obtained from Equation 4.1 as follows.

$$Prob\left[t_{n;1-\alpha/2} < \frac{(\bar{x} - \mu_x)\sqrt{N}}{s} \leq t_{n;\alpha/2}\right] = 1 - \alpha \qquad n = N\text{-}1 \qquad \textbf{(4.3)}$$

Since a certain amount of data has already been collected, the values $\bar{x}$ and s are known. Therefore the above probability statement no longer apply since the quantity $(\bar{x} - \mu_x)\sqrt{N}/s$ either falls into the noted limits (0 or 1) or not. After a sample has been collected the probability statement thus changes as follows.

$$Prob\left[t_{n;1-\alpha/2} < \frac{(\bar{x} - \mu_x)\sqrt{N}}{s} \leq t_{n;\alpha/2}\right] = \begin{Bmatrix} 0 \\ 1 \end{Bmatrix} \qquad \textbf{(4.4)}$$

It is usually not known whether the correct probability is zero or unity. As the value of α becomes small (the interval between $t_{n;1-\alpha/2}$ and $t_{n;\alpha/2}$ becomes larger) the probability is more likely to be unity than zero. If a lot of samples sets were collected and $\bar{x}$ and s computed for each sample, the value in Equation 4.3 should fall within the noted interval for about 1-α of the samples. A statement can thus be made concerning the interval where the quantity $(\bar{x} - \mu_x)\sqrt{N}/s$ would be found with a small degree of uncertainty. These statements are called confidence statements, while the interval associated with this statement is known as the confidence interval. For the case of a mean value estimate, a confidence interval can be established for the mean value μ_x based upon the sample values $\bar{x}$ and s by rearranging the terms in Equation 4.3 as follows.

$$\left[\left(\bar{x} - \frac{st_{n;\alpha/2}}{\sqrt{N}}\right) \leq \mu_x < \bar{x} + \frac{st_{n;\alpha/2}}{\sqrt{N}}\right] \qquad n = N - 1 \qquad \textbf{(4.5)}$$

because $t_{n;1-\alpha/2} = -t_{n;\alpha/2}$. Thus, the true mean value μ_x falls within the stated interval with a confidence of (1- α)100 percent.

As a first iteration, eight, 2 s and four, 4 s measurements were taken for the frequency around 280 Hz. Table 4.1 shows the frequencies.

Table 4.1: Typical third mode frequencies found during a measurement run

Example of 3rd natural frequencies found (2 s samples)				**Example of 3rd natural frequencies found (4 s samples)**	
283.90	283.90	285.09	281.91	279.93	279.74
285.30	285.09	283.70	284.69	280.72	280.52

By using Equation 4.5 in conjunction with the $t_{n;\alpha}$ values found in Bendat and Piersol (1967) and data set found in Table 4.1:

$$\left[\left(\bar{x} - \frac{st_{n;\alpha/2}}{\sqrt{N}}\right) \leq \mu_x < \bar{x} + \frac{st_{n;\alpha/2}}{\sqrt{N}}\right] \qquad n = N - 1$$

furthermore:

$\bar{x}$	=	284.20	
$t_{24;\alpha/2}$	=	2.807	(Bendat and Piersol, 1967 with α=0.995)
s	=	1.12	

Thus one can predict with a 99.5% confidence that the mean value will fall between

$$[282.96 \leq \mu_x < 285.43]$$

This meant a maximum error of 0.87% between sets of measurements and did not fall within the accuracy requirements since a frequency shift of around 0.8% was expected for 5% damage.

Similarly the 99.5% confidence interval for four, 4 s samples can be calculated as

$$[279.57 \leq \mu_x < 280.88]$$

This means a maximum error of 0.47% which was considerably better than the two second samples. Since these were obviously still not accurate enough results, the

data points were increased to 24 for the 2 s samples and 12 for the 4 s intervals. These data sets can be seen in Table 4.2.

Table 4.2: Typical third mode frequencies found during a measurement run

Example of 3rd natural frequencies found (2 s samples)				**Example of 3rd natural frequencies found (4 s samples)**	
283.90	283.50	283.90	284.89	280.52	279.93
283.90	283.70	283.50	284.89	280.52	280.33
281.91	284.69	284.69	285.09	280.72	280.13
284.29	283.70	284.49	283.70	279.93	280.52
284.29	284.69	284.89	285.30	279.93	279.93
283.10	284.69	283.70	285.09	279.74	279.74

Again using Equation 4.5 in conjunction with the $t_{n;\alpha}$ values found in Bendat and Piersol, 1967 and data set found in Table 4.2:

$$[283.73 \leq \mu_x < 284.63]$$

This meant a maximum error of 0.32% between sets of measurements and felt within the accuracy requirements since a frequency shift of around 0.8% was expected for 5% damage.

For 12, 4 s measurements, the 99.5 % confidence interval for the mean value can be calculated in the same way as:

$$[279.88 \leq \mu_x < 280.44]$$

That meant a maximum error of 0.2%. Since this was better than the 24 measurements, and requires roughly the same computational time, it was better to choose 12 sets of 4 seconds.
The fourth mode was also of interest. Since this mode shifted significantly less, it was necessary to check whether 24, 2 s or 12, 4 s measurements were enough.

The data for the fourth mode can be seen in Table 4.3.

Table 4.3: Example of four[illegible]ies found during test run

Example of 4th natural frequencies found (2 s samples)				Example of 4th natural frequencies found (4 s samples)	
446.65	447.28	446.97	446.97	446.97	446.97
446.65	447.28	447.28	446.97	447.28	446.97
446.97	447.59	446.97	446.65	447.28	446.97
446.97	447.28	446.65	447.28	446.97	447.28
446.97	447.28	447.28	446.97	446.97	447.28
446.97	446.97	446.97	446.65	446.97	446.97

Again using the same technique the mean of a measurement set will fall in the range

$$[446.87 \leq \mu_x < 446.87]$$

with a maximum error of 0.07% which was exceptional. For the 12 measurements of 4 s the confidence interval was found to be

$$[446.95 \leq \mu_x < 447.20]$$

giving a maximum error of 0.06%. It is therefore clear that 12, 4 s measurements should give accurate enough results, in order to do damage identification.

Not surprisingly, longer samples of time data gave more accurate results and less were required to achieve an average frequency with a high level of confidence. This was due to the fact that the ARMAX algorithm makes use of a PSD that will be more accurate the longer the length of the time signal used as input. Ideally, an infinitely long time signal would be used which will result in a perfect PSD. This would lead to a perfect fit and the frequency should then not appear to move around a little between measurements. The specific algorithm used was very Random Access Memory (RAM) intensive and long time signals resulted in unrealistic CPU times.

Further experimentation with longer samples was not viable, given the time constraints of the project, but can certainly be looked at in more detail if a decision is made in future to use this technique without modification on actual blades in industry. The confidence interval statistical approach gave a mathematically solid method to determine the number of measurements necessary for a specific sampling length.

4.4 Damage detection measurements

With all the preliminary work done regarding sensor placement, measurement length, signal processing, model fitting and feature extraction, a full set of measurements was taken on a blade.

4.4.1 Measurement system used on the EFBDS

For the damage detection measurements the blade that was to be damaged was instrumented with two piezoelectric strain gauges and one accelerometer. Since the Siglab analyser allows four channels, the remaining channel was used to instrument a different blade to test the ability of the method to predict damage on a specific blade. The location and orientation of the sensors can be seen in Figure 4.15.

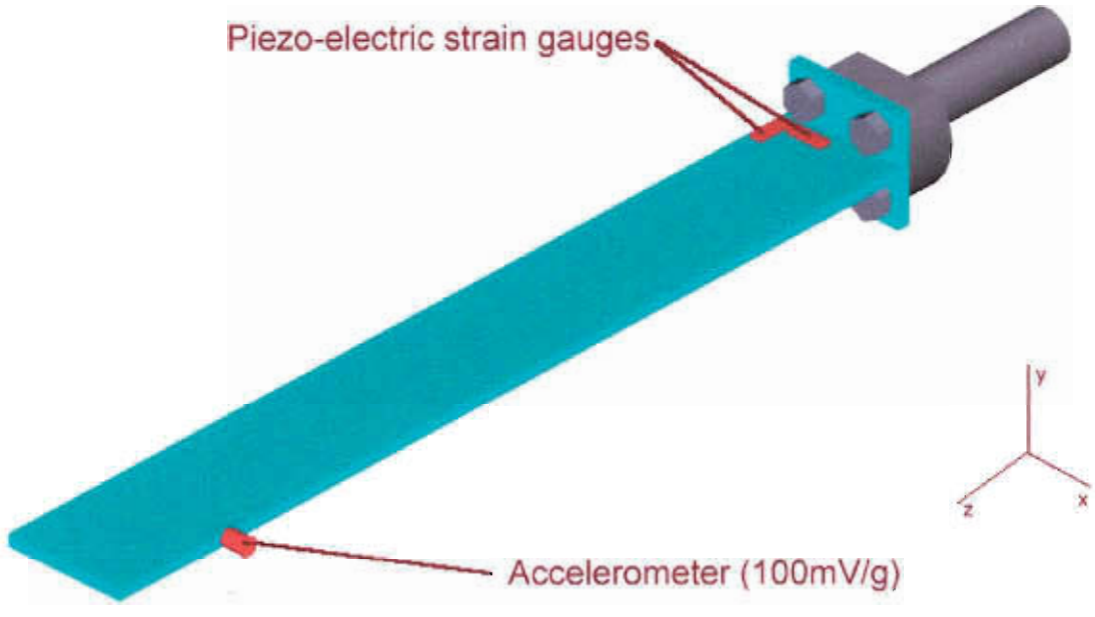

Figure 4.15: Location of sensors on the blade to be damaged

The accelerometer on the undamaged blade was located in the same position as the accelerometer on the blade to be damaged. As discussed in section 4.2.1, both the x-x and the z-z direction show promise for a strain gauge, both were therefore instrumented. The channel numbers can be seen in Table 4.4 along with the calibration values of the sensors associated with each channel.

Table 4.4: Sensor channel and description

Channel number	Sensor type	Sensor sensitivity.
1	Accelerometer (undamaged blade)	103.2mV/g
2	Accelerometer (damaged blade)	9.82mV/g
3	Piezoelectric strain gauge. (x-x)	50mV/μE ± 20%
4	Piezoelectric strain gauge. (z-z)	50mV/μE ± 20%

After a reference set of measurements had been taken, damage was introduced in increments of 10% up to 40%. The damage was introduced by using a thin saw blade and cutting from one side only into the root of the blade.

4.4.2 Result of curve fits

From the finite element work done, the amount by which the frequency should shift is known. The resulting curve fits by the ARMA algorithm for channel 3 with a 500 Hz sampling frequency is shown at various damage levels in Figure 4.16.

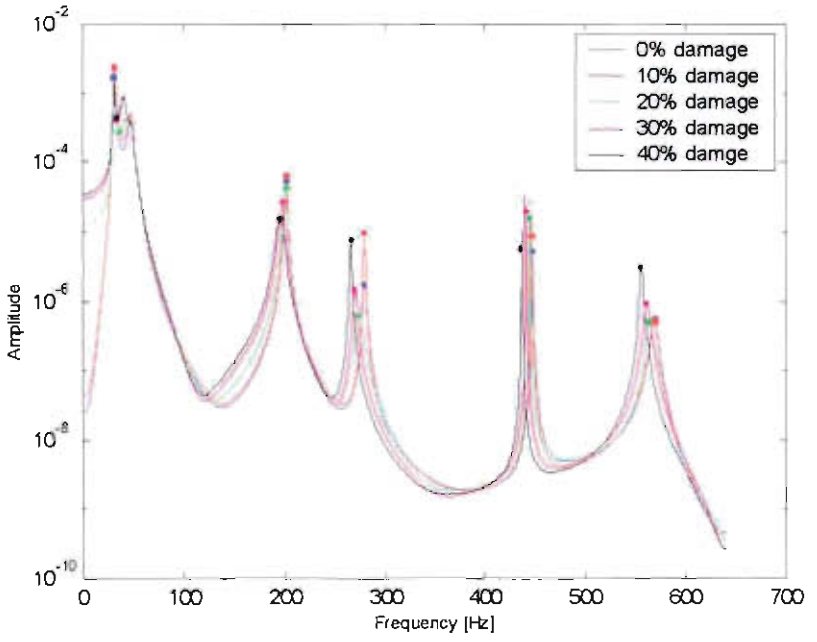

Figure 4.16: ARMA curve fits for channel 3, 500 Hz sampling frequency

It is quite clear that a progressive shift of the natural frequencies can be seen with increasing levels of damage. A waterfall plot of the actual PSDs for the various stages of damage can be seen in Figure 4.17, with a spectrogram of the same set of

measurements in Figure 4.18. The spectrogram in Figure 4.19 shows the ARMAX curve fits.

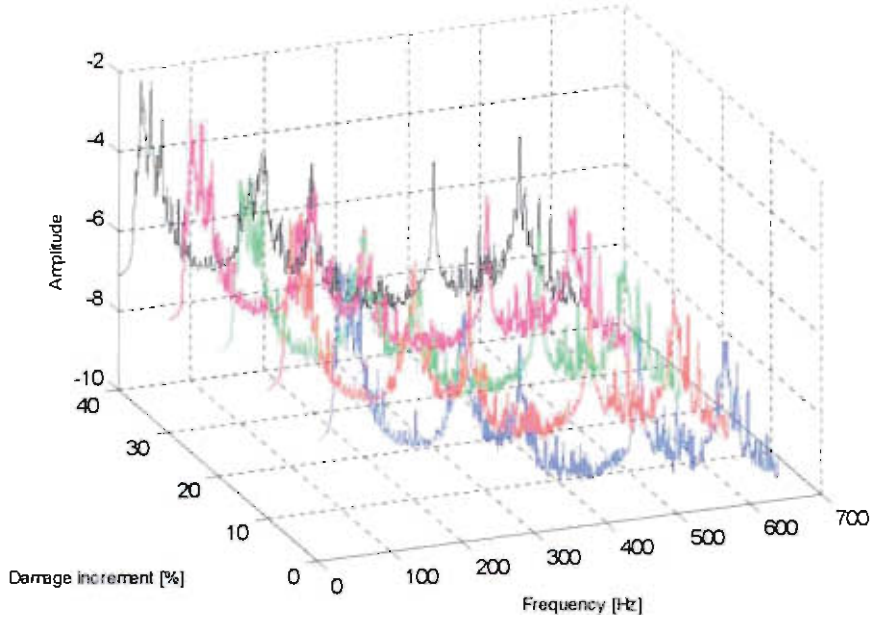

Figure 4.17: Waterfall plot of channel 3, 500 Hz sampling frequency

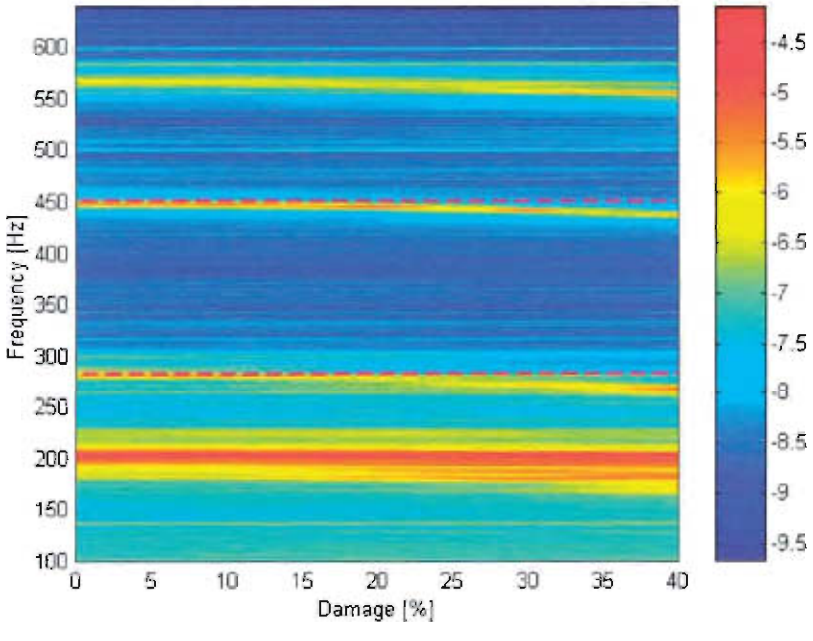

Figure 4.18: Spectrogram showing the frequency shifts with increasing damage

The data in Figure 4.16 to Figure 4.19 is the average of twelve measurement sets of four seconds each. It can thus be stated with a 99.5% confidence that the average of these frequency values will have a measurement error of less than 0.2% for the frequency around 280 Hz, and less than 0.06% for the frequency found around 440 Hz.

Although not very clear in Figure 4.18, the noise floor increases (see Figure 4.17), with increasing levels of damage. This makes physical sense, since the blade cross sectional area gets progressively less, the resultant stress and strain due to the stochastic inputs on the blade should increase (or decrease depending on location of strain gauge relative to crack). This trend can also be seen in the spectrogram plot of the ARMAX curve fits found in Figure 4.19.

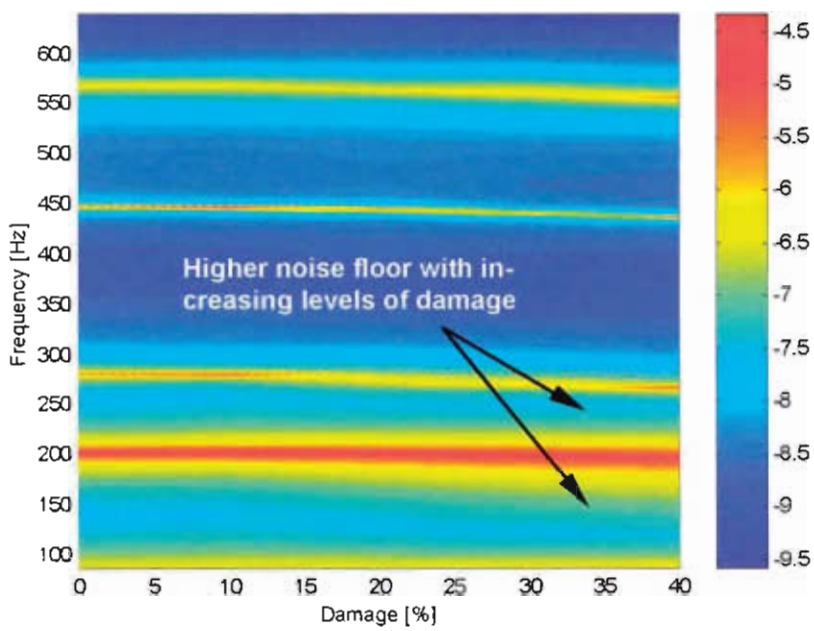

Figure 4.19: Spectrogram of the ARMAX curve fits with increasing levels of damage

The results for a few selected channels and different sampling frequencies are given in appendix D. Table D.1 shows typical results from different channels and taken at different rotational speeds and sampling frequencies for the third natural frequency.

Table D.2 in Appendix D shows the same channels and operating conditions but for the fourth mode shape natural frequency.

It was readily apparent that measurable and significant frequency shifts did take place with increasing damage.

From these examples of measured data, it was apparent that the experimental fan blade damage detector experienced a measurable frequency shift with increasing values of damage. Also immediately obvious was that the frequency shifts for the fourth mode shape was far less than the shifts predicted by the finite element model (see Figure 4.20).

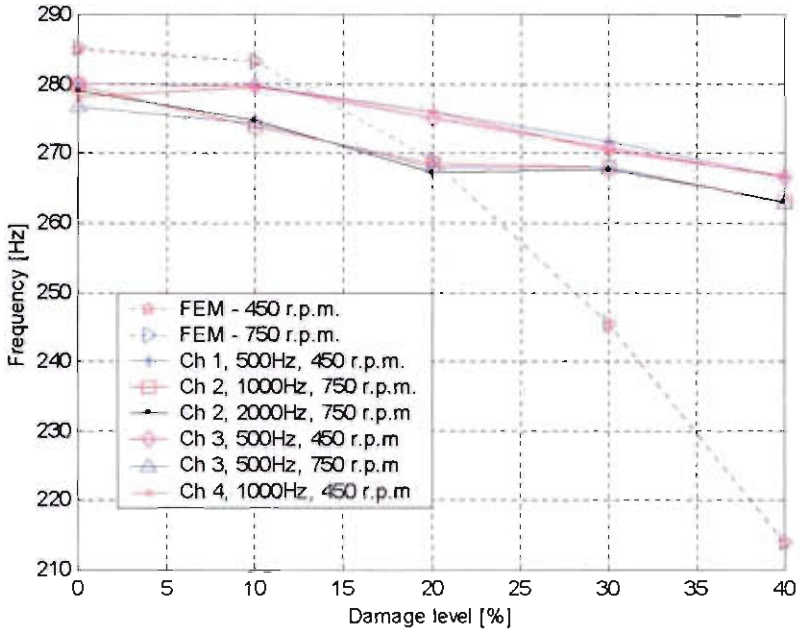

Figure 4.20: Variation of 3rd natural frequency with increasing damage. All samples were 4 s long

The graphs showing the frequency shift per damage increment were directly compiled from the measured data and can be found in Appendix D. Although the general trend of the shifts are the same, the experimental measurements were less sensitive to damage than the finite element model of a single blade predicted. The natural frequency corresponding to the fifth mode shape showed much better correlation however.

As can be seen from Figure 4.20, the measurements sampled at 500 Hz, tended to be more consistent than the measurements sampled at higher frequencies. The reason for this was that the ARMA curve fits, work better when there are less peaks and valleys to find and more consistent fits can be achieved. At higher frequency a large number of redundant poles and zeros need to be used because of the blade pass frequency harmonics and electrical noise. The percentage frequency shift can be seen in Figure 4.21.

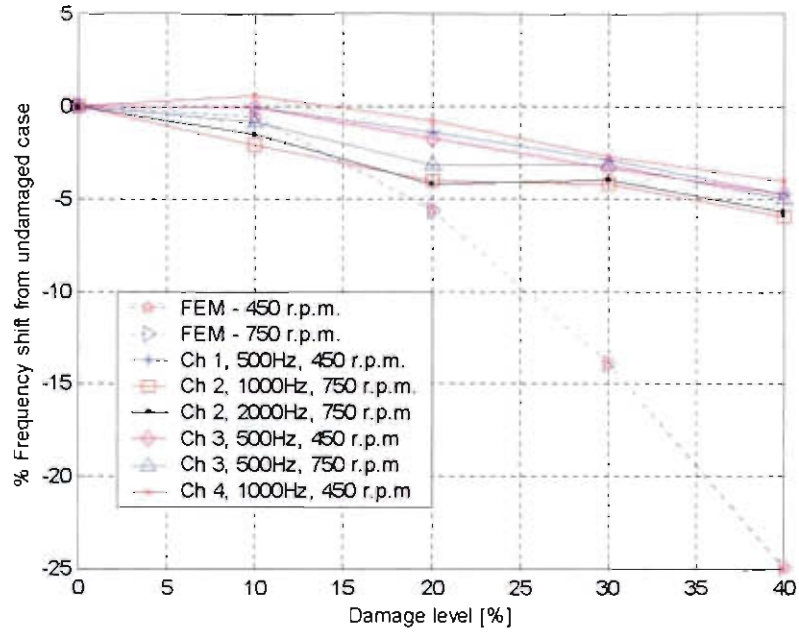

Figure 4.21: Percentage shift from the original undamaged frequency. (280 Hz)

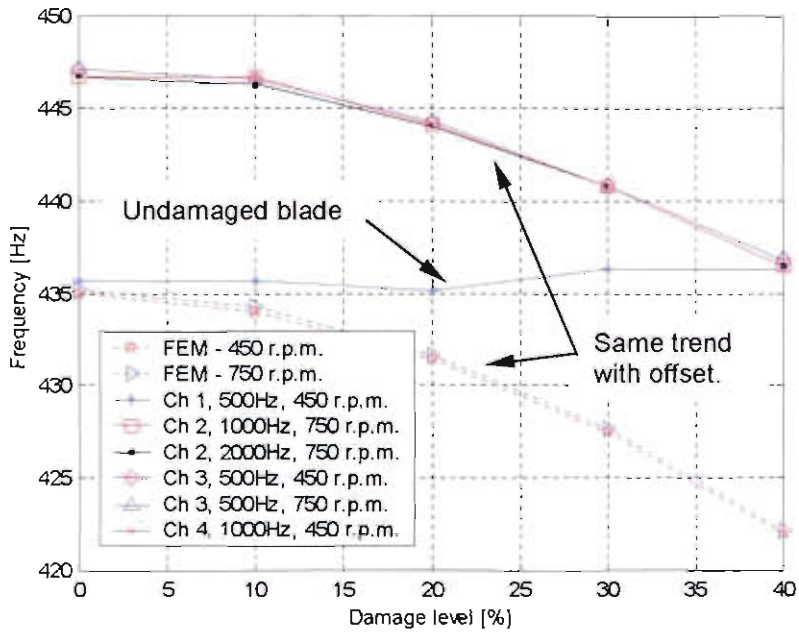

Figure 4.22: Increasing damage levels for the 4th natural frequency

The decrease in the 4th natural frequency can be seen with increasing damage levels in Figure 4.22. The offset of a few Hertz between measurement taken from the un-damaged blade and the damaged blade was not a cause for concern. It was to be expected that the blades would not have the same stiffness at the root of the blade due to the weld used. From FEM it was clear that both the sideways mode shapes

(x-x direction) and the torsional mode shapes were very sensitive to boundary conditions at the root of the blade.

The most significant feature of this mode shape was the lack of shift of the undamaged blade. Although this measurement was influenced to a small extent with increasing levels of damage, no clear pattern could be discerned and the blade would have been classified as healthy.

The percentage change in natural frequencies can be seen in Figure 4.23. Clearly a very good relationship existed between the experimental measurements and the shift predicted by the FEM model for this particular mode shape.

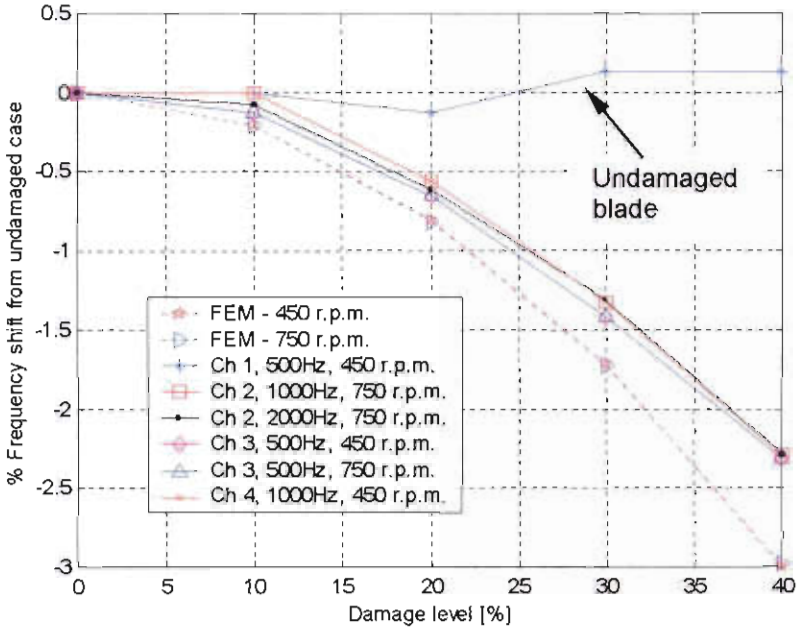

Figure 4.23: Percentage shift of frequency for the fourth mode shape

Although the fourth mode shape showed excellent correlation with predicted FEM results, the third mode shape was not as sensitive to damage as predicted. It was still more sensitive than the fourth mode shape though.

From these results is was clear that further investigation into the discrepancies between the FEM model and the experimental results would have to be done. Chapter 5 deals with this phenomenon.

4.4.3 Time domain damage indicators

Because of the continuing nature of this project with a view to practical implementation on a fan in industry (most likely the FD and ID fans at Majuba), it was decided to investigate other parameters that can be used as features for pattern recognition techniques such as neural networks. Various single values can be calculated for a time signal to give some indication of damage (or other changes). Some of the most important are listed in Heyns (1999).

A. Root mean square (rms)

The *rms* value of a function x(t) over an interval T can be calculated as:

$$X_{rms} = \sqrt{\frac{\int_0^T x(t)^2 dt}{T}} \qquad \textbf{(4.6)}$$

This indicator gives a good indication of changes involving overall peak levels in a signal.

B. Crest factor

This is the ratio of the peak value found to the *rms* level

$$CF = \frac{X_{max}}{X_{rms}} \qquad \textbf{(4.7)}$$

C. Kurtosis

The kurtosis is the fourth statistical moment of a distribution. This value is widely used in machinery diagnostics, particularly for rolling element bearings.

$$kurtosis = \frac{1}{\sigma^4 T}\int_0^T x^4 dt \qquad \textbf{(4.8)}$$

D. Variance and standard deviation

If the mean value is defined as μ_x the variance of data is given by

$$\sigma_x^2 = \lim_{T \to \infty} \frac{1}{T} \int_0^T [x(t) - \mu_x]^2 \, dt$$

The positive square root of the variance is called the standard deviation.

Some examples of the values found can be seen in Figure 4.24 (**V**ariance), Figure 4.25 (*rms*), Figure 4.26 (Kurtosis) and Figure 4.27 (Crest factor)

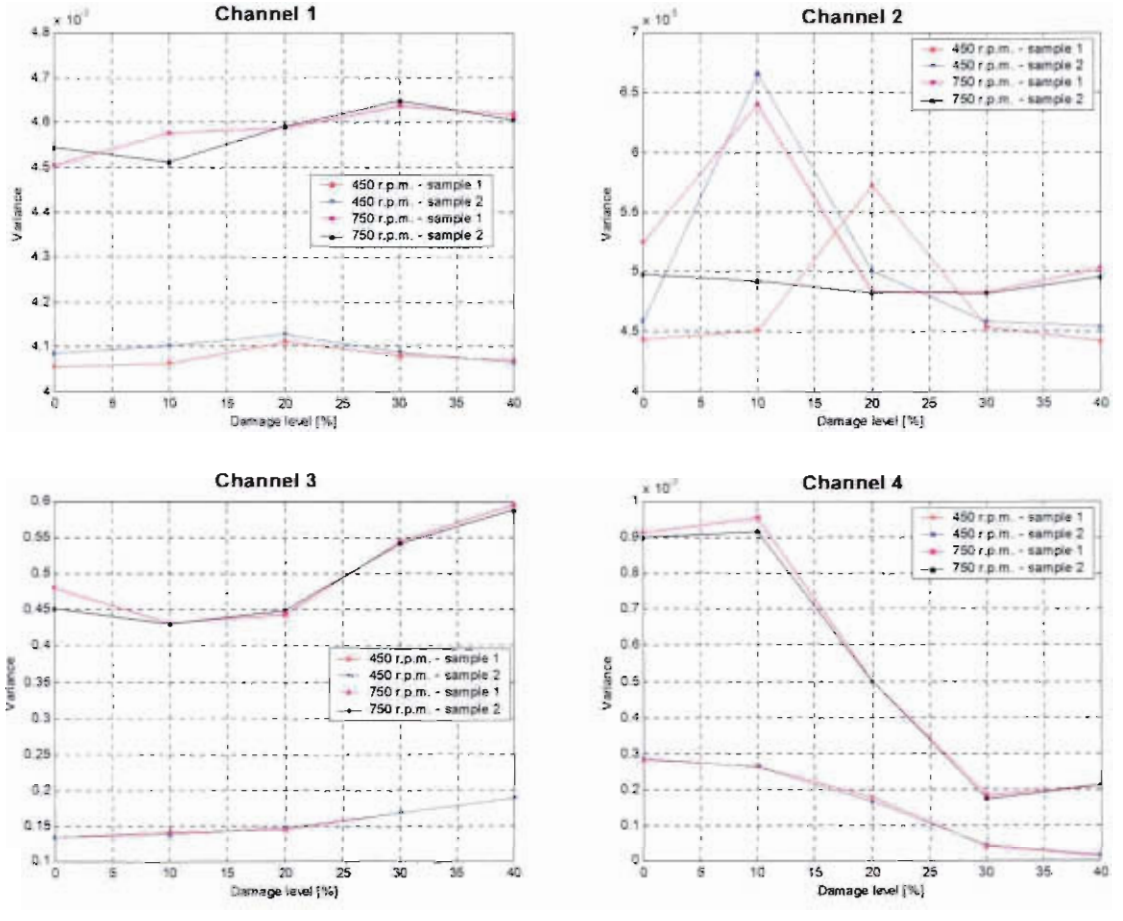

Figure 4.24: Variance plots for channel 1 through 4

Higher rotational speed caused higher stresses in the blade and this could be seen in the higher magnitude values found. Quite clearly the accelerometer channels (1,2) did not measure significantly different signals for increasing levels of damage. This was expected since the movement of the blade will not change significantly with increasing damage. The strain channels (3,4) did show an increase for lower rotational

velocities. This was also expected since the area of undamaged blade (on which the sensor was placed) decreased and the strain therefore increased,.

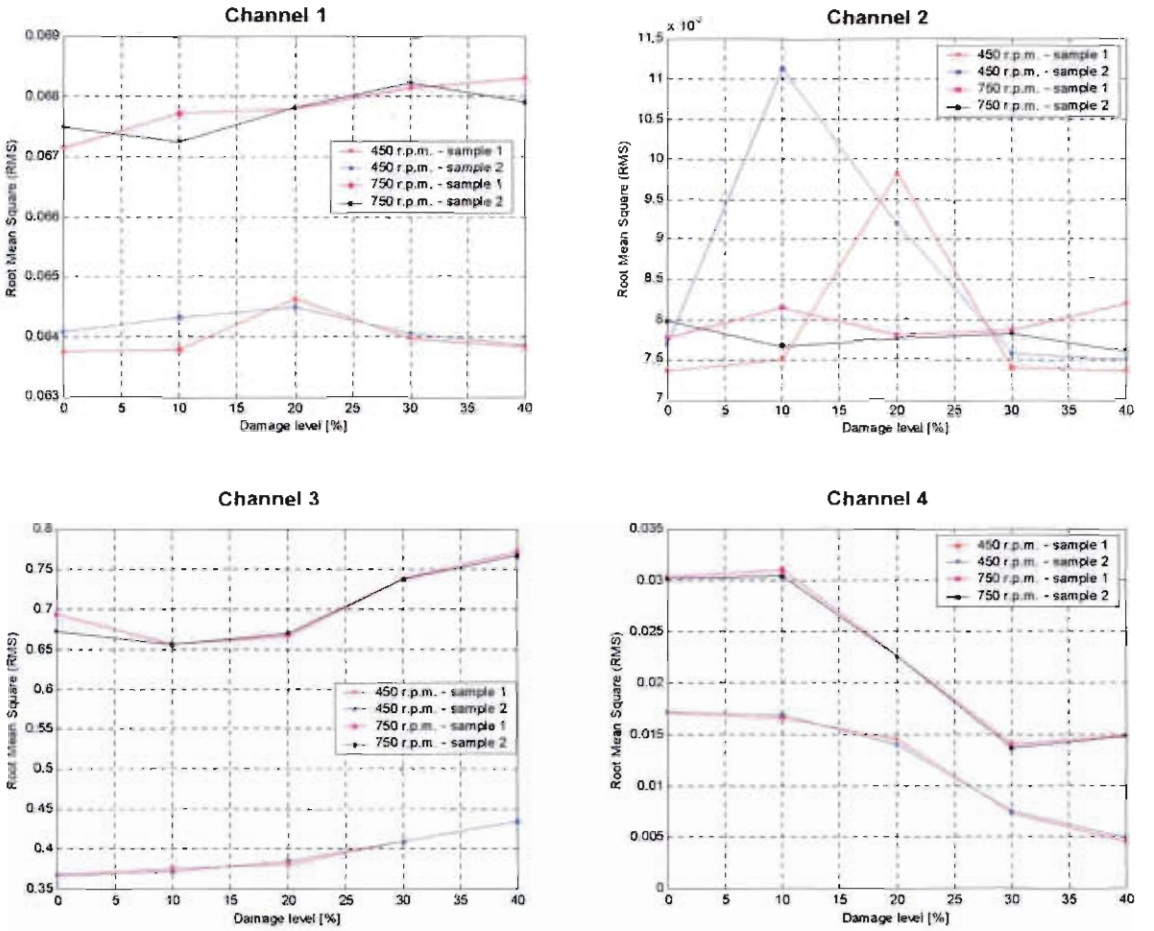

Figure 4.25: Root mean square plots for channel 1 through 4

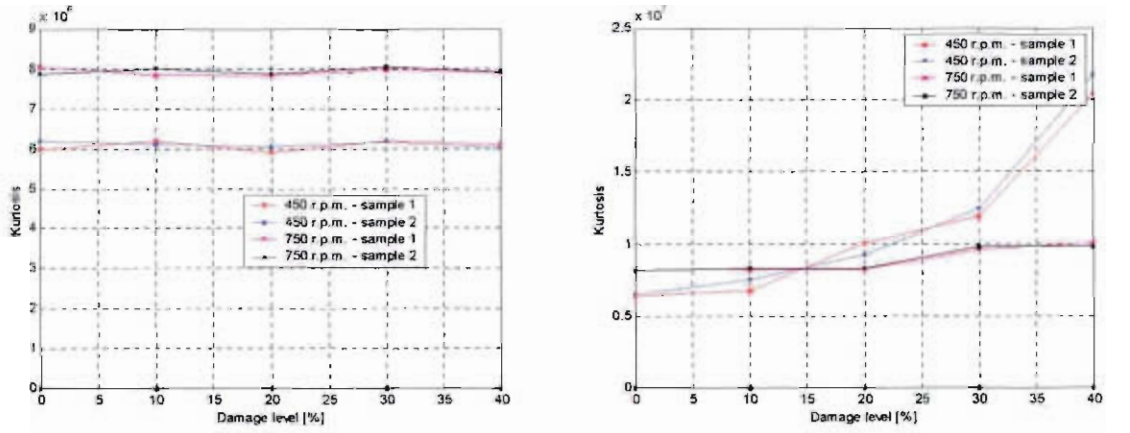

Figure 4.26: Kurtosis plots for channel 3(left) and channel 4(right)

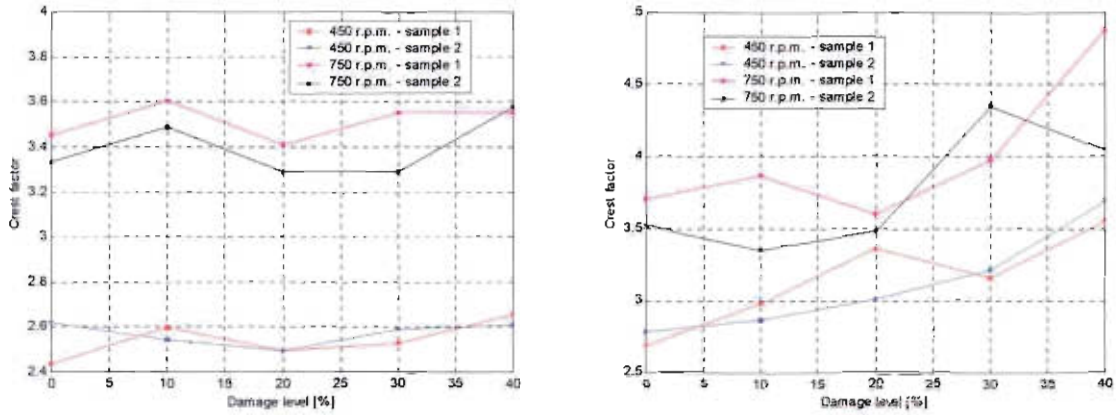

Figure 4.27: Crest factor plots for channel 3(left) and channel 4(right)

Clearly only some of the strain gauge measurements can be used with some success as a damage indicator at specific operational conditions. A better option would probably be to use these time domain indicators in conjunction with the ARMAX models to predict the amount of damage on a blade. This could make very good features for use in Self Organising Maps (SOM) or neural networks.

4.5 Conclusions

Although the ARMAX algorithm used made use of time domain data to generate a polynomial model, the end result was frequency domain parameters. The shift of natural frequencies proved to be a good damage indicator when the approximate location of damage is known. As discussed in Chapter 1, cracks will typically only originate at the root of fan blades because of the location of maximum stress. The results obtained are especially good if results of various researchers over the years (as discussed in Chapter 1) are taken into account.

Some discrepancies were found between the FEM and experimental results for the third mode shape. This phenomenon was investigated in Chapter 5.

Time domain damage indicators did not provide a clear indication or trend with increasing levels of damage for most operating conditions and sensors. If only some of these values are used as features in a pattern recognition algorithm such as a neural network it may further improve the prediction accuracy, especially if a whole range of features (more features were discovered in Chapter 5) are used.